Desalination and Water Treatment
www.deswater.com

doi:10.5004/dwt.2016.0239

59 (2017) 220–229
January

Removal of methylene blue from aqueous solution by ceramsite filter media combined with high temperature calcination for regeneration

Tianpeng Li[a], Tingting Sun[b], Dengxin Li[a,*]

[a]*College of Environment Science and Engineering, Donghua University, Shanghai 201620, PR China, Tel. +86 2167792541; Fax: +862167792522; emails: tianpeng985@126.com (T. Li), lidengxin@dhu.edu.cn (D. Li)*
[b]*Institute of Neuroscience and Anatomy, Zhejiang University School of Medicine, Hangzhou 310058, PR China, email: ttsun@zju.edu.cn*

Received 1 March 2016; Accepted 18 June 2016

ABSTRACT

Ceramsite, made of municipal waste, was prepared by high-temperature sintering process. Ceramsite was utilized as a filter media for the removal methylene blue (MB) from aqueous solution and was regenerated by high temperature calcination. The batch studies results showed that the equilibrium isotherms and adsorption kinetics of MB adsorption on ceramsite filter media (CFM) were described better by the Langmuir model and pseudo-first-order kinetics than by the Freundlich model and pseudo-second-order kinetics, respectively. Under the CFM bed column operating conditions of the MB initial concentration of 5 mg L^{-1}, particle size of 0.5 ± 0.2 mm and flow rate of 1 mL min^{-1}, the breakthrough data were agreed well with the bed depth service time (BDST) model at 15% and 50% breakthrough for MB. The regeneration tests proved that high-temperature calcination was an effective regeneration method for the recovery of exhausted CFM. Both the adsorption kinetics of MB on CFM and regenerated CFM (in a certain cycle range) were found to match the Thomas model; whereas, the maximum adsorption capacity of CFM decreased slightly with the increase in regeneration cycles.

Keywords: Methylene blue dye; Ceramiste filter media; Adsorption equilibrium isotherm; Thomas model; Regeneration

1. Introduction

Dyes are essentially colored substances capable of imparting their color to other substances. Various kinds of dyes are used extensively as coloring substances in textiles, dyestuff, plastics, rubber, paper and related industries [1]. It has been estimated that approximately 15% of the dyes were lost during the dyeing process and were discharged in the form of pollutants in the effluent [2]. Dye wastewater possesses a high COD concentration, low biodegradability, large amount of suspended solids, broadly fluctuating pH and strong color [3]. The discharge of dye wastewater into the environment, particularly aquatic environment, causes considerable environmental pollution [4,5], probably due to the following factors: firstly, the sewage contains complex aromatic molecular structure possibly originating from coal tar-based hydrocarbons, such as benzene, anthracene, toluene, naphthalene and xylene, which make them more stable. Secondly, the sewage is colorful even at very low concentrations, giving undesirable color to the water, reducing sunlight penetration and resisting photochemical and biological attacks. Thirdly, the degradation products of the sewage are toxic, mutagenic, carcinogenic and they also result in increasing the COD, NH_4^+-N and BOD levels of aquatic sources. Therefore, it is imperative that before discharge, dye wastewater must be treated and cleaned by an ecological and cost effective process.

Nowadays, various technologies have been employed for the treatment of dye wastewater, including coagulation-flocculation [6], fouling resistant nanofiltration and reverse osmosis membranes [7], heterogeneous Fenton oxidation [8], sequencing batch reactor (SBR) method [9] and

*Corresponding author.

some other processes [10–12]. Among the above methods, filtration is the preferred method because of its simplicity, high efficiency, less secondary pollution (such as toxic and harmful intermediates, excess sludge) and their potential in renewability [13,14]. To achieve better treatment performance, the selection of a suitable filter media is critical in filtration design and operation [15].

A number of researchers have reported that there were several materials such as novel clay ceramic particles (CCPs) [16], intermittently operated slow sand filtration (ISSF) [17], decolorizing ceramsites [18] and multilayer glassy microporous filter [19], can be used as filter medias. Unfortunately, there are still some shortcomings for practical application of these materials; for example, sand, clay and natural zeolite are mineral resources, which do not meet with the requirements of sustainable development. Furthermore, considering rigorous ecological and commercial demands for sustainability, repeated reuse of filter media is one of the most important parameters for routine applications [20,21].

Ceramsite, with high porosity, large specific surface area, low bulk and apparent density, is commonly used as building material as well as filter media in water/wastewater treatment [22,23]. Traditionally, natural resources were used as main raw materials to prepare ceramsite. For the purpose of reusing of municipal wastes and approaching the object of treating waste with waste at the same time, some alternate municipal wastes can be used, for example, sludge, fly ash and river sediment as they can be treated as natural substitutes for producing ceramsite as filter media. This research will provide a prospective pathway for municipal wastes utilization.

Keeping this in mind, the widely used methylene blue (MB) dye was chosen as our target model pollutant. In this study, the characterization of CFM was characterized. By means of batch adsorption tests, the equilibrium isotherms and adsorption kinetics of MB adsorption on CFM were conducted. Column studies were carried out in CFM bed column runs. At last, the exhausted CFM was regenerated by high temperature calcination, and its regeneration performance was evaluated.

2. Materials and methods

2.1. Preparation of CFM

The composition of raw materials is shown in Table 1. The general preparation process of CFM is illustrated in Fig. 1. For the preparation of CFM, sludge, fly ash and river sediment were mixed with a mass ratio of 5:1:4 to form the ceramsite specimen, the necessary amount of deionized water was added to the mixture to obtain adequate plasticity, green bodies were produced manually and their shape were spherical, with an average diameters of 10 mm. Then, the green bodies were placed at room temperature until they dried completely. After drying they were sintered in a pipe furnace (model SX2-6-13, Shanghai Y-feng, Co., Ltd, China) in air atmosphere, the sintering temperatures and sintering times are mentioned in details in Fig. 2(a). Finally, the CFM was crushed down and sieved to be desired diameters. The filtered CFM was then washed several times until the washed water no longer to be colored or turbid, After this the CFM was dried for 120 min at 60°C and was then preserved under dry conditions for further use.

2.2. Batch study

A stock solution of 500 mg L^{-1} was prepared by dissolving an appropriate quantity of MB (cationic dye,

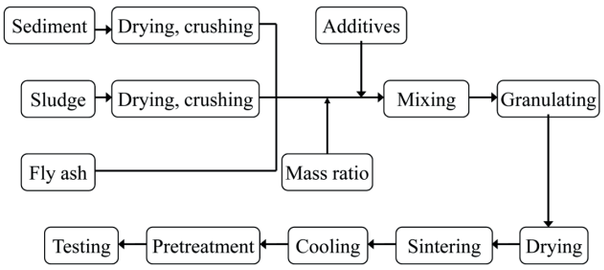

Fig. 1. Preparation process of CFM.

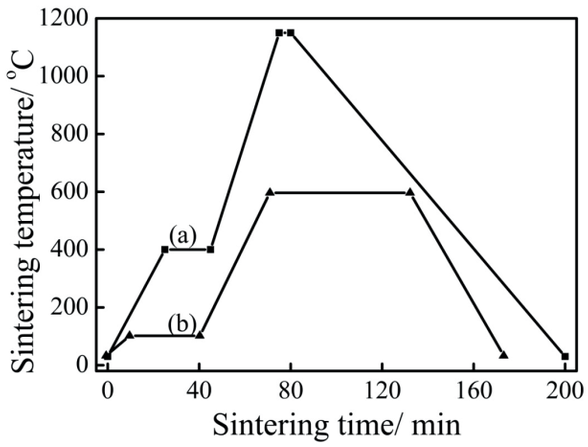

Fig. 2. Temperature controls of (a) sintering process of CFM and (b) sintering regeneration of exhausted CFM.

Table 1
The composition of raw materials (%) [24]

Raw materials	SiO_2	Al_2O_3	Fe_2O_3	CaO	MgO	Na_2O	K_2O	Ignition loss
Sludge	7.5	2.3	6.9	2.9	0.5	0.1	0.5	72.4
River sediment	52.5	17.6	5.1	1.5	1.8	0.5	2.8	8.5
Fly ash	56.8	25.7	7.0	8.1	0.8	0.4	1.9	0.2

$C_{16}H_{18}ClN_3S{\cdot}3H_2O$, *Mwt*: 373.88 g mol^{-1}, analytical grade, Sinopharm Chemical Reagent Co., Ltd, China) in deionized water. All test solutions at the desired concentrations were prepared by successive dilutions to obtain the required initial experimental concentration. Deionized water was used in all experiments. These experiments were carried out at ambient temperature. The batch experiment procedure was as follows: a beaker having 100 mL of MB solution was placed on a magnetic stirrer (200 rpm) and 2 g CFM (particle size = 0.5 ± 0.2 mm) was added into this solution. At given time intervals, the concentration of MB in the filtrate was measured. All of the experiments were performed twice under the same conditions and an averaged value was employed.

2.3. Column study

The laboratory-scale experimental set-up used in the study is presented in Fig. 3. A fixed particle size of CFM was prepared and filled in two cleaned cylindrical glass tubes of 53 cm effective height × 3.5 cm internal diameter. At the bottom of each glass tube, a filter paper was placed in order to avoid the penetration of CFM. On the top of each glass tube, a filter paper was placed as barrier to prevent CFM from spilling out. The dye inlet was fed into the column from the bottom of one tube with a variable speed peristaltic pump (model BT300-02, Baoding Qili Precision Pump Co., Ltd, China). The effluent was discharged from the top of the other one tube by outlet pipe connected to a collecting tank. Started time was defined as the point when the effluent was discharged. After a designated time, the concentration of MB in the filtrate was measured.

2.4. Regeneration experiments

The exhausted CFM was collected and calcined in a pipe furnace in air atmosphere, the regeneration temperatures and regeneration times are mentioned in details in Fig. 2(b). After regeneration, CFM was cooled down to room temperature. Subsequently, the CFM was washed several times to remove any impurities, and dried for 120 min at 60°C. And then, the column studies of the regenerated CFM were carried out, according to the methods mentioned in Section 2.3.

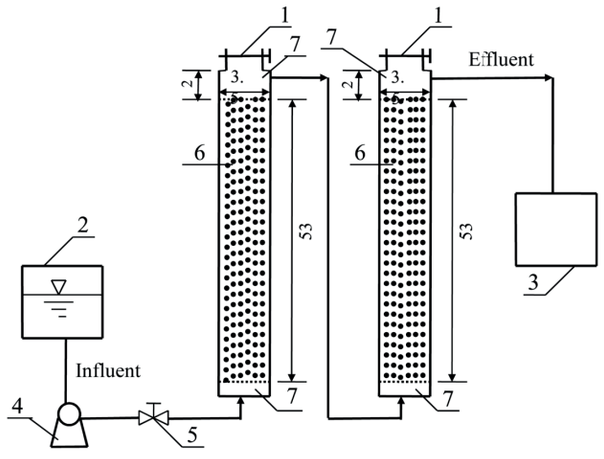

Fig. 3. Schematic diagram of experimental set-up (dimensioning unit: cm): 1-feed inlet/discharge port; 2-feedwater tank; 3-collecting tank; 4-peristaltic pump; 5-flow-meter; 6-CFM; and 7-buffer zone.

2.5. Analytical methods

The composition of raw materials was measured by X-ray fluorescence spectrometry (XRF, model XRF-1800, Shimadzu Corporation, Japan); physical properties of CFM were determined according to China's industry standard (Artificial Ceramsite Filter Material for Water Treatment, CJ/T 299-2008); contents of metal elements in lixivium of CFM were measured according to the previous research method [25]; the surface morphology and crystalline phases of CFM were assessed by Scanning Electron Microscope-Energy Dispersive Spectrometer (SEM-EDS, model Quanta- 250, Fei Instrument, Czech) and X-ray diffraction (XRD, model D/max- 2550 PC, Rigaku, Japan), respectively; the Brunauer-Emmett-Teller (BET) surface area calculated from N_2 adsorption and desorption measurements obtained using fully automatic specific and micro pore size analyzer (model AUTOSORB-IQ2-MP, USA); the MB concentration was measured using a UV-Vis spectrophotometer (model UV754N, INESA analytical instrument Co., Ltd, China) at its maximum wavelength of 664 nm. The adsorption capacity of CFM at t min (q_t, mg g^{-1}) and at equilibrium (q_e, mg g^{-1}) were calculated by Eqs. (1) and (2):

$$q_t = \frac{(C_0 - C_t)V}{m} \tag{1}$$

$$q_e = \frac{(C_0 - C_e)V}{m} \tag{2}$$

where C_0, C_t and C_e are the concentrations of MB in solution at starting, time t and equilibrium, respectively, mg L^{-1}. V is the volume of the working solution (L) and m is the mass of CFM (g).

3. Results and discussion

3.1. Characterization of CFM

3.1.1. Physical properties

The measurements of every item for each physical property were repeated three times, and the mean value was used as mentioned in Table 2. It was clearly demonstrated that the several essential physical properties of CFM, including breaking and wear rate, solubility in hydrochloric acid, silt carrying capacity, void fraction and BET surface area were in accordance with the China's industry standard (CJ/T 299-2008).

As seen in Fig. 4, the chemical compositions of the CFM included various metal oxides and metal compounds, such as syn-Fe_2O_3, Quartz-SiO_2, Chromium Vanadium Oxide, Albite, Labradorite and Anorthite, they all attributed to the raw material composition. Meanwhile, low-content heavy

metal compounds were also observed, such as $Cr(VO_4)$. In order to determine the lixiviation of metals in the water, especially heavy metals, lixiviation test was carried out to know more about the metal elements and the potential toxicity of the CFM. As Table 3 suggested, only few heavy metals, such as Cr, Zn and Cu, were found in the lixivium, and found to be much lower than the threshold levels as per the China standards, that is, GB 5085.3-2007. The reason for this is that during sintering process, metals, mostly derived from raw materials, were solidified into the glassy phase in the form of metallic oxides except some that were volatilized at high temperature [16].

From above findings, we could come to the conclusion that the self-made CFM presented a promising application for wastewater treatment. Other researchers, such as Zhao et al. [22] and Xu et al. [26], also obtained the similar conclusion.

Table 2
Physical properties of CFM {24}

Parameters	Value	Threshold[a]
Breaking and wear rate	0.2	≤6
Solubility in hydrochloric acid	0.01	≤2
Silt carrying capacity	0.2	≤1
Void fraction	71.1	>40
BET surface area ($\times 10^4$)	0.73	>0.5

[a]China's industry standard of CJ/T 299-2008; parameters except for surface area ($cm^2\ g^{-1}$) are in %.

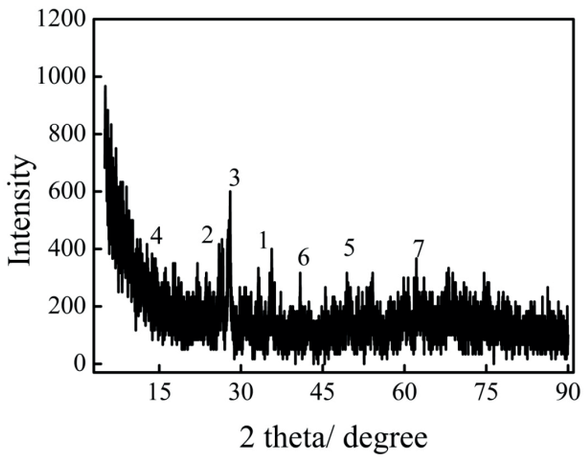

Fig. 4. XRD pattern of CFM (1: Hematite, 2: Quartz-SiO_2, 3: Albite, Ca-rich; 4: Labradorite-$Ca_{0.64}Na_{0.35}(Al_{1.63}Si_{2.37}O_8)$; 5: Albite low-$Na(AlSi_3O_8)$; 6: Anorthite-$Ca(Al_2Si_2O_8)$; 7: Chromium Vanadium Oxide).

Table 3
Contents of metal elements in lixivium of CFM (mg kg^{-1})

Metal elements	Content in lixivium	Threshold[a]
Cr	≤0.15	5.0
Zn	0.29	100.0
Cu	≤0.15	100.0
Al	0.052	NM
Fe	ND	NM
Ca	10.03	NM
Mg	2.065	NM
Na	4.631	NM
K	ND	NM

[a]Identification standards for hazardous wastes-identification for extraction toxicity of China (GB5085.3-2007); ND = not detected; NM = not mentioned.

3.1.2. Pore characteristics and surface morphology

As Fig. 5(a) showed that the surface of CFM was rough with many small pores, which achieved suitable specific surface area, porosity and aperture size. From Fig. 5(b), it was found that the cross-section of CFM was porous and with relatively large pores. These rough surface and porous properties of CFM have close relation to their chemical constituents. The unique porous characteristics and surface morphology of CFM guaranteed that the wastewater can flow evenly, thus providing the high removal efficiency and this is also consistent with other researches [27]. As seen in Fig. 5(a) and (b), the EDS results revealed that the species of chemical elements in surface and cross section were highly consistent, including C, O, Na, Al, Si, Ca and Fe. Conversely, there were some differences in the contents weightage (wt%) and atomic percentage of chemical elements. Compared with surface, the contents weightage (wt%) and atomic percentage of O, Na and Si in cross-section decreased, while the Ca and Fe amount increased significantly (>two times).

Moreover, mineralogical analyses of CFM were carried out using XRD (Fig. 4). It was noted that the XRD pattern of CFM has major peaks assigned to (1) syn-Fe_2O_3, (2) SiO_2 and (3) $(Na, Ca)Al(Si, Al)_3O_8$, as well as

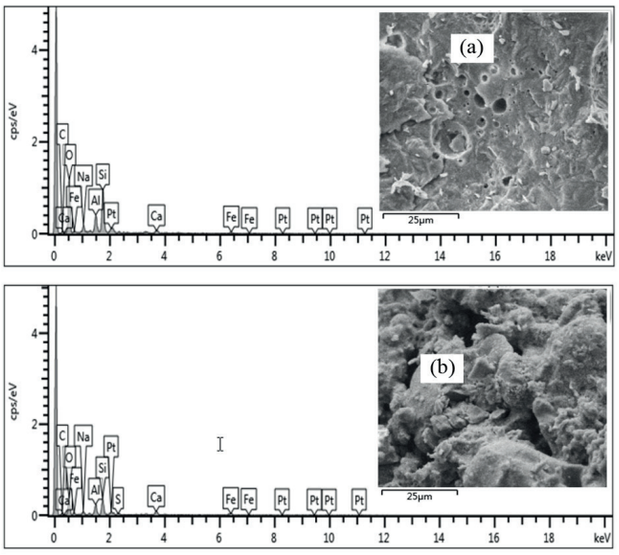

Fig. 5. SEM photographs and EDS spectra of CFM: (a) surface and (b) cross-section.

minor peaks assigned to (4) $Ca_{0.64}Na_{0.35}(Al_{1.63}Si_{2.37}O_8)$, (5) $Na(AlSi_3O_8)$ and (6) $Ca(Al_2Si_2O_8)$. Fig. 4 also reflected that the CFM has two kinds of chemical compositions: one is glassy materials, such as SiO_2 and (Na, Ca)Al(Si, Al)$_3O_8$, which are major components of ceramsite, forming the ceramsite framework; the other is flux oxides, such as syn-Fe_2O_3 and CaO, which lower the melting point of the glassy phase. Besides, some researchers discovered that CFM also has gasogenic constituents [28], which generate gaseous bubbles bloating the body of ceramsite, including carbon, ferric oxide, ferrous oxide and magnetic iron.

3.2. Batch study

3.2.1. Equilibrium isotherms

Equilibrium data, known as adsorption isotherms, are important in the basic design of adsorption systems, and are critical in optimizing the use of adsorbents. Generally, Langmuir and Freundlich models are used for explaining monolayer homogeneous adsorption processes and modeling the adsorption on heterogeneous surfaces, respectively [29]. In this study, both the models were selected to evaluate for experimental results. Their linear model equations are expressed by Eqs. (3) and (4), respectively:

$$\frac{C_e}{q_e} = \frac{1}{Mk} + \frac{C_e}{M} \tag{3}$$

$$\log q_e = \log k_f + \frac{1}{n}\log C_e \tag{4}$$

where M is the maximum monolayer adsorption capacity (mg g^{-1}), C_e is the equilibrium concentration of the solution (mg L^{-1}), 1/n is the heterogeneity factor, k (L mg^{-1}) and k_f (mg g^{-1}) are the Langmuir and Freundlich equilibrium constants, respectively.

The fitted liner plots of the Langmuir and Freundlich models of MB adsorption on CFM after stirred for 240 min were analyzed, and the results are illustrated in Fig. 6. The results determined that the equilibrium isotherm data were aligned to the linear Langmuir and Freundlich models at the concentration of MB ranging from 5 to 20 mg L^{-1}. The Langmuir model provided a slightly more consistent fit to the data (Fig. 6(a), R^2 = 0.9988) as compared with the Freundlich model (Fig. 6(b), R^2 = 0.9601). That is, the former model provided a better description of the process than the latter, suggesting that the adsorption of MB on CFM was a monolayer homogeneous adsorption process. Furthermore, according to the Langmuir model equation (Fig. 6(a)), the maximum monolayer adsorption capacity of CFM was 0.603 mg g^{-1} after stirred for 240 min.

3.2.2. Adsorption kinetics

In order to explore the adsorption mechanism of CFM for MB, characteristic constants of adsorption were determined using pseudo-first-order and pseudo-second-order reaction kinetics [30]. Their simple linear equations correspond to Eqs. (5) and (6), respectively:

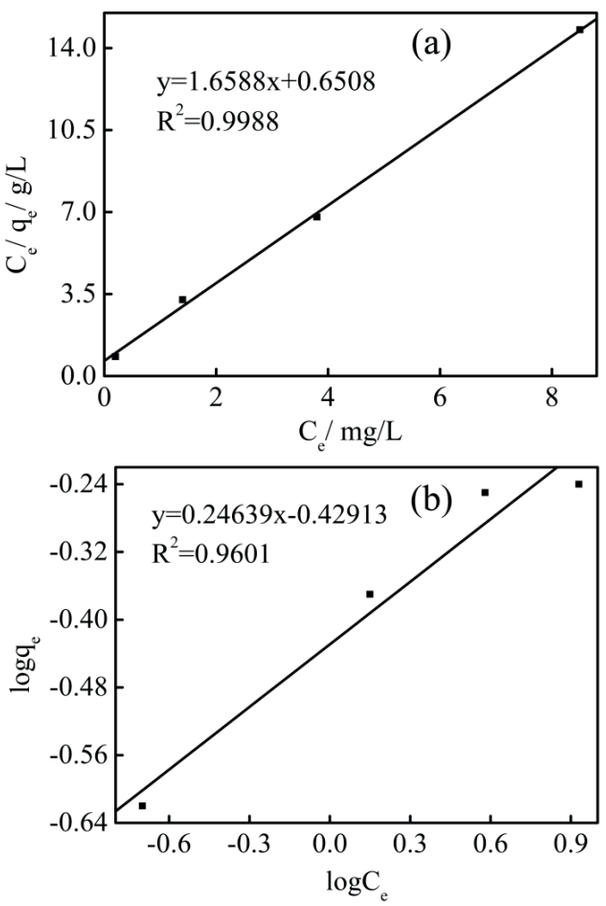

Fig. 6. Linear plots of (a) Langmuir isotherm and (b) Freundlich isotherm of MB adsorption on CFM.

$$\ln(q_e - q_t) = \ln q_e - k_1 t \tag{5}$$

$$\frac{t}{q_t} = \frac{1}{k_2 q_e^{\,2}} + \frac{t}{q_e} \tag{6}$$

where k_1 and k_2 are the rate constants of the pseudo-first and pseudo-second-order reaction kinetics, respectively, g min·mg^{-1}.

The kinetic parameters of pseudo-first and pseudo-second-order reactions for the removal of MB from aqueous solution by CFM are summarized in Table 4. While comparing the correlation coefficients (R^2) listed under Table 4, it was found that the adsorption of MB on CFM could be described well by the pseudo-first-order kinetic model, which has a higher correlation coefficient value (R^2 > 0.989) at the concentration of MB ranging from 5 to 20 mg L^{-1}. On the contrary, the adsorption of MB on CFM could not be fitted by the pseudo-second-order kinetic model, owing to poor correlation coefficient values.

Table 4
Kinetic parameters for the removal of MB from aqueous solution by CFM

C_0 (mg L^{-1})	Pseudo-first-order kinetic			Pseudo-second-order kinetic		
	q_e (mg g^{-1})	$k_1 \times 10^{-3}$ (min^{-1})	R^2	q_e (mg g^{-1})	$k_2 \times 10^{-3}$ (g mg·min^{-1})	R^2
5	0.293	13.6	0.9921	0.466	10.7	0.9662
10	0.511	10.4	0.9929	1.328	1.6	0.859
15	0.711	11.1	0.9896	4.755	0.1364	0.1991
20	0.68	9.2	0.9941	6.236	0.0742	0.0946

3.3. Column study

3.3.1. Effect of initial concentration

The effect of initial concentration on MB removal by CFM was carried out by varying the initial concentrations from 5 to 25 mg L^{-1}. As observed from Fig. 7(a), the breakthrough curve of the lower initial concentration of 5 mg L^{-1} tend to be more gradual, meaning that the column was difficult to be completely exhausted. On the contrary, when the initial concentrations were more than 5 mg L^{-1}, the breakthrough curves became steeper gradually. The breakthrough times and the exhausting times for the initial concentrations of 5, 10, 15, 20 and 25 mg L^{-1} were obtained as 335, 155, 65, 65 and 35 min and 665, 575, 455, 395 and 335 min, respectively. Thus, the MB concentration of 5 mg L^{-1} was chosen as the initial concentration to investigate the effect of other factors on removal efficiency. The observed decrease in breakthrough time and exhaustion time at higher initial concentration may be due to the rapid exhaustion of the sorption sites of adsorbent [31].

3.3.2. Effect of particle size

The variation of MB removal by CFM with operating time was assessed as a function of particle sizes of CFM in the range of 0.5–11 mm and the results are shown in Fig. 7(b). With the increase in particle sizes from 0.5 to 11 mm and prolonged operating time, the breakthrough curves became increasingly steep. The breakthrough points for the particle sizes of 0.5, 1, 5, 8 and 11 mm were got at 335, 185, 125, 65 and 35 min, respectively, and the exhausting times also were obtained at 665, 635, 545, 485 and 425 min, respectively. Therefore, the particle size of CFM for removal MB was selected 0.5 mm.

A typical N_2 adsorption-desorption isotherms of CFM with different particle sizes were studied, and the results are presented in Fig. 8. The figure revealed that both the samples showed type IV isotherms with H_2-type hysteresis loop at P/P_0 = 0.45–0.95, and the isotherms showed high absorption at high relative pressure P/P_0 = 0.99. It was evident that the BET surface area of CFM particle size of 0.5 mm was much larger than that of CFM particle size of 5 mm. Moreover, each sample exhibited a similar type of H_2-type hysteresis loop suggesting that pore size and shape were basically same in both samples. Reports have demonstrated that the smaller of particle size of adsorbent, the more efficiency of adsorbate removal. This is probably due to large surface area resulting in high dispersion, outstanding stability and high loading capacity [32].

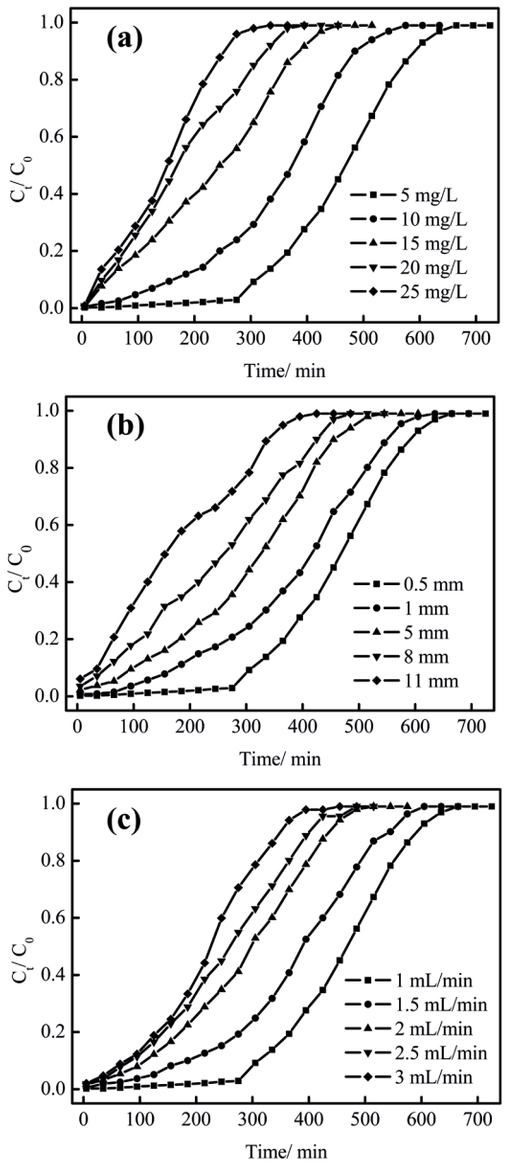

Fig. 7. Effect of (a) initial concentration (particle size = 0.5 mm and flow rate = 1.0 mL min^{-1}), (b) particle size (±0.2 mm, initial concentration = 5 mg L^{-1} and flow rate = 1.0 mL min^{-1}) and (c) flow rate (initial concentration = 5 mg L^{-1} and particle size = 0.5 mm) on breakthrough curves of MB removal from aqueous solution with the CFM bed depth of 106 cm.

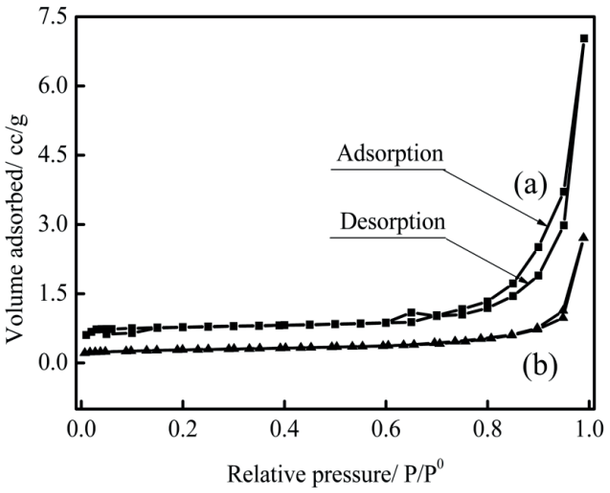

Fig. 8. BET surface area calculated from N_2 adsorption-desorption isotherms for (a) CFM particle size of 0.5 mm and (b) CFM particle size of 5 mm.

3.3.3. Effect of flow rate

The effect of flow rates were investigated at the speed of 1, 1.5, 2, 2.5 and 3 mL min^{-1}, and the results are depicted in Fig. 7(c). This figure illustrates that increase in the flow rates resulted with a decrease in MB removal efficiency. The breakthrough times for the flow rates in the range of 1–3 mL min^{-1} presented a decreasing trend from 335 to 65 min and the exhausting times also decreased from 665 to 455 min. Thereby, 1 mL min^{-1} was finally selected as a feasible flow rate. The reasons for this change may be attributed to the fact that at high flow rates the contact time between the adsorbent and adsorbate became shorter, reducing the removal efficiency. On the other hand, the movement of adsorption zone along the bed is faster, reducing the removal efficiency as well.

3.3.4. Effect of bed height

Fig. 9(a) displayed the breakthrough curves of the bed heights of 26.5, 53, 106 and 159 cm at the CFM bed column operating conditions of the MB initial concentration of 5 mg L^{-1}, particle size of 0.5 mm and flow rate of 1 mL min^{-1}. As expected, the breakthrough times and exhausting times increased with increasing bed height. Decreasing the bed height caused the breakthrough curves become steeper, resulting in the early exhaustion of the CFM bed.

The original work on the BDST model was developed by Bohart and Adams [33], they proposed a relationship between bed height (H) and the time (t) taken for breakthrough to occur. The BDST model is based on the assumption that the rate of sorption is controlled by the surface reaction between the sorbate and the residual capacity of the sorbent [34]. Later, Hutchins modified of the BDST model with a linear relationship as follows [35]:

$$t_b = \frac{N_A}{C_0 V} H - \frac{1}{k_A C_0} \ln\left(\frac{C_0}{C_b} - 1\right) \quad (7)$$

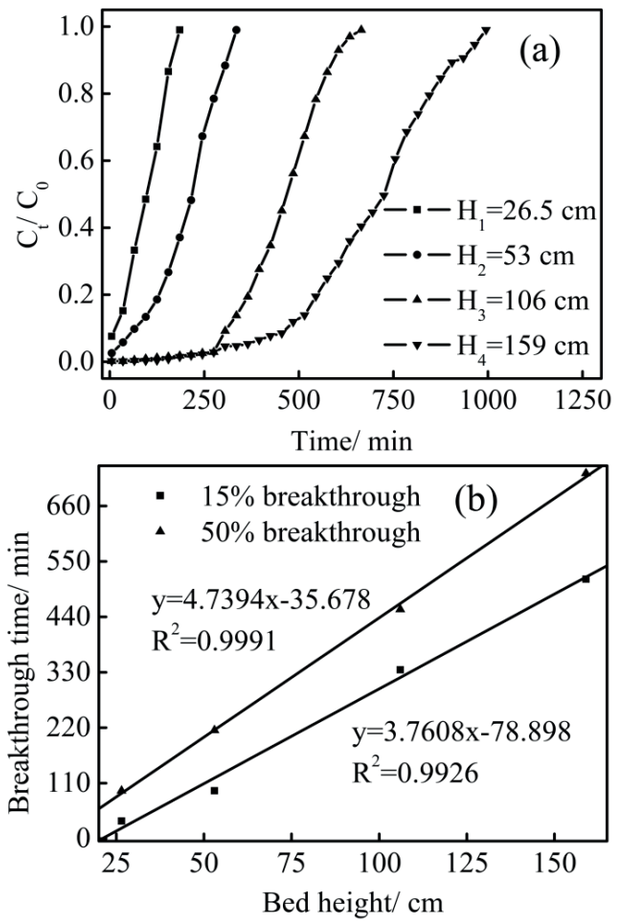

Fig. 9. (a) Effect of bed heights on breakthrough curves of MB removal from aqueous solution and (b) bed height vs. service time at 15% and 50% breakthrough for MB.

where C_0 and C_b are the initial and desired concentration of MB at breakthrough, respectively, mg L^{-1}; k is the sorption rate constant of the column (L mg·min^{-1}); N_0 is the sorptive capacity of the CFM bed column (mg L^{-1}); H is the height of the CFM bed (cm); V is the linear flow velocity of the feed to the bed (mL min^{-1}); and t is the service time of column under above conditions (min).

Eq. (7) can be rewritten in the form of a straight line:

$$t_b = mH + n \quad (8)$$

where m is the slope of Eq. (7) ($m = N_A/C_0V$) and n is the intercept of Eq. (7) represented as Eq. (9).

$$n = -\frac{1}{k_A C_0} \ln\left(\frac{C_0}{C_b} - 1\right) \quad (9)$$

Fig. 9(b) illustrated the bed height vs. service time for the removal of MB on the CFM bed column at 15% and 50% breakthrough. According to Fig. 9(b), the sorptive capacity (N_0) of the CFM bed column at 15% and 50% breakthrough for MB were 18.804 and 23.697 mg L^{-1}, respectively. High

correlation coefficients ($R^2 > 0.99$) explained that the variation of the service times with the bed heights was highly linear for both the breakthroughs (Fig. 9(b)). Thus, indicating the validity of the BDST model when applied to the continuous CFM column studies.

3.4. Regeneration performance

For real applications, the reusability and reproducibility is a very important and crucial factor to obtain an advanced and efficient filter media as the dyes can be recovered and the filter media can be regenerated for next applications. An excellent filter media should not only possess high removal efficiency but should also possess strong regeneration capacity, which may significantly reduce the overall cost of the adsorbent [36,37]. The importance of regeneration processes has stimulated intense research and therefore, a wide variety of regeneration techniques for exhausted materials have been proposed, such as chemical methods, wet air oxidative (WAO) treatment, high-temperature calcination, and electrochemical methods. Among them, high-temperature calcination is considered as the most cost-effective method [38,39].

Herein, high-temperature calcination was employed to regenerate the exhausted CFM, and the results are shown in Fig. 10. It was indicated that the breakthrough point obtained at 335 min for the original CFM (0 cycle) and at 305, 305, 305 and 275 min for regenerated CFM in 1st, 2nd, 3rd and 4th cycles, respectively. Compared with third and fourth regeneration CFM, the breakthrough curves of changing tendency of first and second regeneration CFM and original CFM were similar. The reason is that as the increasing number of regeneration cycles, the CFM became more and more resistant towards the heat treatment [40]. Also, a part of primary porosity decreased as the micropores were blocked during recycles. The results demonstrate that the CFM can be considered as a reusable material with excellent regeneration behavior for the removal of MB from aqueous solution in a certain cycle range.

In general, the Thomas model is applied to determine the maximum adsorption capacity (q_{max}, mmol g^{-1}) of an adsorbent, which is necessary to design of an adsorbent column. The model is based on the Langmuir adsorption/desorption, no axial dispersion and the rate driving force follows second order reversible reaction kinetics [41,42]. The model equation is listed as:

$$\frac{C_t}{C_0} = \frac{1}{1+\exp\left(\frac{k_{Th}q_{max}m}{v} - k_{Th}C_0 t\right)} \quad (10)$$

where k_{Th} is the Thomas rate constant (mL mmol min^{-1}), v is the volumetric flow rate (mL min^{-1}) and m is the mass of CFM in the column (g).

The linearized form of the Thomas model is presented by:

$$\ln\frac{C_t}{C_0 - C_t} = k_{Th}C_0 t \quad \frac{k_{Th}q_{max}m}{v} \quad (11)$$

The values of k_{Th} and q_{max} were obtained from the $\ln C_t/(C_0–C_t)$ vs. operating time (t) by fitting the experimental data (Fig. 10), and the results are presented in Table 5. It was reflected that the adsorption of MB on CFM could be described well by the Thomas model, with a high correlation coefficient (R^2 = 0.9801) and a strong adsorption capacity (q_{max} = 0.48 mmol g^{-1}). Table 5 also indicated that the adsorption of MB on the regenerated CFM followed the Thomas model. The values of q_{max} of regenerated CFM in 1st, 2nd, 3rd and 4th cycles declined by 4.2%, 8.3%, 16.7% and 18.8%, respectively. As the number of cycles increased, the values of correlation coefficient decreased. Our results confirm that the high-temperature calcination method was suitable for regeneration of the exhausted CFM, without impacting the adsorption capacity of CFM column in a certain cycle range.

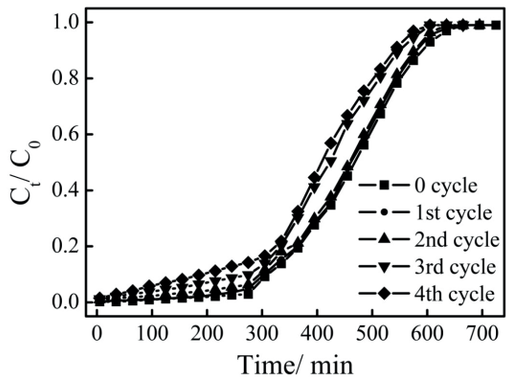

Fig. 10. Effect of regeneration of CFM on breakthrough curves of MB removal from aqueous solution under the initial concentration = 5 mg L^{-1}, particle size = 0.5 mm, flow rate = 1 mL min^{-1} and the CFM bed depth = 106 cm.

Table 5
Parameters of the Thomas model under different regeneration cycles using linear regression

Cycles	$k_{Th} \times 10^{-3}$ (mL $mmol^{-1}$ min^{-1})	q_{max} (mmol g^{-1})	R^2
0	3.1	0.48	0.9801
1	3.0	0.46	0.9761
2	2.72	0.44	0.9422
3	2.7	0.4	0.9403
4	2.6	0.39	0.9374

Note: C_0 = 5 mg L^{-1}, v = 1 mL min^{-1}, m = 4,620 g.

4. Conclusions

A laboratory-scale experiment was designed to investigate the removal efficiency of MB from aqueous solution by the self-made CFM, and coupled with high temperature calcination for regeneration. The main conclusions extracted from this study may be summarized as follows:

(1) The physical properties and the concentrations of metals in lixivium of the self-made CFM meet with the requirements of CJ/T 299-2008 and GB 5085.3-2007 (China Standards), respectively, suggesting

that the CFM is a suitable and safe filter material for wastewater treatment.

(2) Compared with the pseudo-second-order kinetics and Freundlich model, the batch adsorption data are described well by the pseudo-first-order kinetics and Langmuir model, with higher values of correlation coefficient ($R^2 > 0.989$ and $R^2 = 0.9988$, respectively).

(3) Under the CFM bed column operating conditions of MB initial concentration of 5 mg L^{-1}, CFM particle size of 0.5 ± 0.2 mm and flow rate of 1 mL min^{-1}, at 15% and 50% breakthrough for MB, the breakthrough data are agreed well with the BDST model.

(4) The process of MB adsorption on CFM follows the Thomas model closely, without being influence by the regeneration cycle (in a certain cycle range). These results demonstrate that the high-temperature calcination is a preferable method for exhausted CFM regeneration.

Overall, the novel CFM has a great potential to be used as an environmental friendly adsorbent for wastewater treatment, with efficient adsorption process and strong adsorption capacity, as well as good regeneration performance.

Acknowledgments

We thank the Fundamental Research Funds for the Central Universities of China (Project No. 15D111321) and "Textile Light" Application Basic Research of China (Project No. J201503).

References

[1] Z.H. Chen, J.W. Fu, M.H. Wang, X.Z. Wang, J.A. Zhang, Q. Xu, Adsorption of cationic dye (methylene blue) from aqueous solution using poly (cyclotriphosphazene-co-4,4′-sulfonyldiphenol) nanospheres, Appl. Surf. Sci., 289 (2014) 495–501.

[2] Y. Liu, J.J. Li, Y. Yang, B.P. Li, Facile immobilization of polyaspartate onto silica gels via poly (dopamine) for the removal of methylene blue from aqueous solution, Appl. Surf. Sci., 351 (2015) 831–839.

[3] R. Subramaniam, S.K. Ponnusamy, Novel adsorbent from agricultural waste (cashew NUT shell) for methylene blue dye removal: optimization by response surface methodology, Water Resour. Ind., 11 (2015) 64–70.

[4] M. Soniya, G. Muthuraman, Comparative study between liquid–liquid extraction and bulk liquid membrane for the removal and recovery of methylene blue from wastewater, J. Ind. Eng. Chem., 30 (2015) 266–273.

[5] S. Jafari, F.P. Zhao, D.B. Zhao, M. Lahtinen, A. Bhatnagar, M. Sillanpää, A comparative study for the removal of methylene blue dye by N and S modified TiO_2 adsorbents, J. Mol. Liq., 207 (2015) 90–98.

[6] Y.X. Wei, A.M. Ding, L. Dong, Y.Q. Tang, F.L. Yu, X.Z. Dong, Characterisation and coagulation performance of an inorganic coagulant-poly-magnesium-silicate- chloride in treatment of simulated dyeing wastewater, Colloid. Surf. A: Physicochem. Eng. Aspects, 470 (2015) 137–141.

[7] I.C. Kim, K.H. Lee, Dyeing process wastewater treatment using fouling resistant nanofiltration and reverse osmosis membranes, Desalination, 192 (2006) 246–251.

[8] B.M. Esteves, C.S. Rodrigues, R.A. Boaventura, F.J. Maldonado-hodar, L.M. Madeira, Coupling of acrylic dyeing wastewater treatment by heterogeneous Fenton oxidation in a continuous stirred tank reactor with biological degradation in a sequential batch reactor, J. Environ. Manage., 166 (2016) 193–203.

[9] S. Sathian, M. Rajasimman, C.S. Rathnasabapathy, C. Karthikeyan, Performance evaluation of SBR for the treatment of dyeing wastewater by simultaneous biological and adsorption processes, J. Water Process Eng., 4 (2014) 82–90.

[10] S. Vajnhandl, A.M.L. Marechal, Ultrasound in textile dyeing and the decolouration/mineralization of textile dyes, Dyes Pigments, 65 (2005) 89–101.

[11] E.L. Hu, X.B. Wu, S.M. Shang, X.M. Tao, S.X. Jiang, L. Gan, Catalytic ozonation of simulated textile dyeing wastewater using mesoporous carbon aerogel supported copper oxide catalyst, J. Clean. Prod., 112 (2016) 4710–4718.

[12] X. Cai, B. Zhang, L. Shi, H.D. Liu, J.L. Zhang, L.H. Huang, S.Z. Tan, Study the photocatalysis activity of hydrothermal-synthesized $BiVO_4$-graphene composite on methylene blue, Desal. Water Treat., 57 (2016) 6365–6371.

[13] B.W. Yang, Q. Chang, C. He, Y. Zhang, Wettability study of mineral wastewater treatment filter media, Chem. Eng. Process., 46 (2007) 975–981.

[14] C.J. Hsu, S.S. Hsiau, A study of filtration performance in a cross-flow moving granular bed filter: the influence of gas flow uniformity, Powder Technol., 274 (2015) 20–27.

[15] F. Zhao, F.F. Weng, G. Xue, Q.R. Jiang, Y.P. Qiu, Filtration performance of three dimensional fabric filter in a membrane bioreactor for wastewater treatment, Sep. Purif. Technol., 157 (2016) 17–26.

[16] W. Han, Q.Y. Yue, S.Q. Wu, Y.Q. Zhao, B.Y. Gao, Q. Li, Y. Wang, Application and advantages of novel clay ceramic particles (CCPs) in an up-flow anaerobic bio-filter (UAF) for wastewater treatment, Bioresour. Technol., 137 (2013) 171–178.

[17] M.W. Jenkins, S.K. Tiwari, J. Darby, Bacterial, viral and turbidity removal by intermittent slow sand filtration for household use in developing countries: experimental investigation and modeling, Water Res., 45 (2011) 6227–6239.

[18] X.L. Guo, Y.D. Yao, G.F. Yin, Y.Q. Kang, Y. Luo, L. Zhuo, Preparation of decolorizing ceramsites for printing and dyeing wastewater with acid and base treated clay, Appl. Clay Sci., 40 (2008) 20–26.

[19] O. Şan, C. Özgür, Wastewater filtration performance of multilayer glassy microporous filters, Ceram. Int., 37 (2011) 3425–3430.

[20] K. Lu, X.L. Zhang, Y.L. Zhao, Z.L. Wu, Removal of color from textile dyeing wastewater by foam separation, J. Hazard. Mater., 182 (2010) 928–932.

[21] D. Dutta, D. Thakur, D. Bahadur, SnO_2 quantum dots decorated silica nanoparticles for fast removal of cationic dye (methylene blue) from wastewater, Chem. Eng. J., 281 (2015) 482–490.

[22] Y.Q. Zhao, Q.Y. Yue, R.B. Li, M. Yue, S.X. Han, B.Y. Gao, Q. Li, H. Yu, Research on sludge-fly ash ceramic particles (SFCP) for synthetic and municipal wastewater treatment in biological aerated filter (BAF), Bioresour. Technol., 100 (2009) 4955–4962.

[23] Q.Y. Yue, S.X. Han, M. Yue, B.Y. Gao, Q. Li, H. Yu, Y.Q. Zhao, Y.F. Qi, The performance of biological anaerobic filters packed with sludge-fly ash ceramic particles (SFCP) and commercial ceramic particles (CCP) during the restart period: effect of the C/N ratios and filter media, Bioresour. Technol., 100 (2009) 5016–5020.

[24] T.P. Li, T.T. Sun, D.X. Li, Preparation, sintering behavior and expansion performance of ceramsite filter media from dewatered sewage sludge, coal fly ash and river sediment, J. Mater. Cycles Waste Manag., DOI:10.1007/s10163-016-0547-3.

[25] S.X. Han, Q.Y. Yue, M. Yue, B.Y. Gao, Q. Li, H. Yu, Y.Q. Zhao, Y.F. Qi, The characteristics and application of sludge-fly ash ceramic particles (SFCP) as novel filter media, J. Hazard. Mater., 171 (2009) 809–814.

[26] G.R. Xu, J.L. Zou, G.B. Li, Ceramsite obtained from water and wastewater sludge and its characteristics affected by $(Fe_2O_3+CaO+MgO)/(SiO_2+Al_2O_3)$, Water Res., 43 (2009) 2885–2893.

[27] Y. Zhang, F. He, S.B. Xia, L.W. Kong, D. Xu, Z.B. Wu, Adsorption of sediment phosphorus by porous ceramic filter media coated with nano-titanium dioxide film, Ecol. Eng., 64 (2014) 186–192.

[28] J.A. Cusidó, L.V. Cremades, M. González, Gaseous emissions from ceramics manufactured with urban sewage sludge during firing processes, Waste Manage., 23 (2003) 273–280.

[29] R.J. Umpleby, S.C. Baxter, Y.Z. Chen, R.N. Shah, K.D. Shimizu, Characterization of molecularly imprinted polymers with the Langmuir-Freundlich isotherm, Anal. Chem., 73 (2001) 4584–4591.
[30] K.R. Raven, A. Jain, R.H. Loeppert, Arsenite and arsenate adsorption on ferrihydrite: kinetics, equilibrium, and adsorption envelopes, Environ. Sci. Technol., 32 (1998) 344–349.
[31] O. Ozdemir, M. Turan, A.Z. Turan, A. Faki, A.B. Engin, Feasibility analysis of color removal from textile dyeing wastewater in a fixed-bed column system by surfactant-modified zeolite (SMZ), J. Hazard. Mater., 166 (2009) 647–654.
[32] A.K. Dutta, S.K. Maji, B. Adhikary, γ-Fe_2O_3 nanoparticles: an easily recoverable effective photo-catalyst for the degradation of rose bengal and methylene blue dyes in the waste-water treatment plant, Mater. Res. Bull., 49 (2014) 28–34.
[33] V.K.C. Lee, J.F.P. And, G. Mckay, Development of fixed-bed adsorber correlation models, Ind. Eng. Chem. Res., 39 (2000) 2427–2433.
[34] V.C. Srivastava, B. Prasad, I.M. Mishra, I.D. Mall, M.M. Swamy, Prediction of breakthrough curves for sorptive removal of phenol by bagasse fly ash packed bed, Ind. Eng. Chem. Res., 47 (2008) 1603–1613.
[35] J.L. Sotelo, G. Ovejero, A. Rodríguez, S. Álvarez, J. García, Removal of atenolol and isoproturon in aqueous solutions by adsorption in a fixed-bed column, Ind. Eng. Chem. Res., 51 (2012) 5045–5055.
[36] L. Zhou, J.C. Huang, B.Z. He, F.A. Zhang, H.B. Li, Peach gum for efficient removal of methylene blue and methyl violet dyes from aqueous solution, Carbohyd. Polym., 101 (2014) 574–581.
[37] Q. Zhou, Q. Gao, W.J. Luo, C.J. Yan, Z.N. Ji, P. Duan, One-step synthesis of amino-functionalized attapulgite clay nanoparticles adsorbent by hydrothermal carbonization of chitosan for removal of methylene blue from wastewater, Colloid. Surf. A: Physicochem. Eng. Aspects, 470 (2015) 248–257.
[38] C.T. Murunaka, C. Julcour, A.M. Wilhelm, H. Delmas, C.A.O. Nascimento, Regeneration of activated carbon by (photo)-Fenton oxidation, Ind. Eng. Chem. Res., 49 (2010) 989–995.
[39] S. Román, B. Ledesma, J.F. González, A. Al-Kassir, G. Engo, A. Álvarez-Murillo, Two stage thermal regeneration of exhausted activated carbons: steam gasification of effluents, J. Anal. Appl. Pyrol., 103 (2013) 201–206.
[40] B. Ledesma, S. Román, A. Álvarez-Murillo, E. Sabio, J.F. González, Cyclic adsorption/thermal regeneration of activated carbons, J. Anal. Appl. Pyrol., 106 (2014) 112–117.
[41] F. Rozada, M. Otero, A.I. García, A. Morán, Application in fixed-bed systems of adsorbents obtained from sewage sludge and discarded tyres, Dyes Pigments, 72 (2007) 47–56.
[42] M. Ghasemi, A.R. Keshtkar, R. Dabbagh, S.J. Safdari, Biosorption of uranium (VI) from aqueous solutions by Ca-pretreated cystoseira indicaalga: breakthrough curves studies and modeling, J. Hazard. Mater., 189 (2011) 141–149.